INTERNATIONAL JOURNAL OF MARITIME TECHNOLOGY
IJMT Vol.18/Spring & Summer 2023 (58-69)
Available online at: www. ijmt.ir

Eulerian-Lagrangian Study of Bubble Collision on Pressure Distribution due to Cloud Cavitation Collapse

Ali Katoozi [1], Miralam Mahdi [2*]

[1] *Master of Science, Mechanical Engineering Department, Shahid Rajaee Teacher Training University, Tehran, Iran, katoozi.a@gmail.com*
[2] *Associate Professor, Mechanical Engineering Department, Shahid Rajaee Teacher Training University, Tehran, Iran, m.mahdi@sru.ac.ir*

ARTICLE INFO

Article History:
Received: 24 Dec 2021
Accepted: 28 Jun 2023

Keywords:
Bubble collision
Cavitation flow
Erosion intensity
Eulerian-Lagrangian method
Bubble dynamics

ABSTRACT

In this study, to numerically investigate the consequence of bubble collision on the pressure distribution due to cavitation collapse, the bubble behavior around NACA0015 2D hydrofoil has been simulated using the Eulerian-Lagrangian perspective. Macroscopic examination of the cavitation flow was determined by the homogeneous mixture model (Eulerian method) and the bubble motion path based on the applied forces using Newton's second law and the development of numerical code (Lagrange method). Bubble oscillations were obtained from the modified Rayleigh-Plesset-Keller-Herring equation. To study the effect of bubbles colliding (bubble with wall and bubble with the bubble), the model of vertical elastic forces and vertical and tangential viscosities used by Heitkam et al. To pair the obtained results and solve them, the fourth-order Runge-Kutta method with variable time step has been used, which has increased the data solving speed up to 10 times. From the Keller& Kolodner relationship, a pressure wave emitted from the collapse of a spherical bubble and the model of Soyama et al, the total energy of the cavitation-induced shocks, which is the result of the accumulation of all the shocks on each other, is obtained. The results showed that the effects of increasing the radius by decreasing the cavitation number are the same, when the bubble colliding with the wall is applied and when it is not and by decreasing the cavitation number, the bubble growth rate increases, and by increasing the bubble radius, the erosion intensity increases. The process of bubble growth starts earlier in the case of collision with the wall than in the case in which the collision did not occur, therefore, the cavitation number has little effect in this case and is related to the impact effects. The result of the impact of the bubble on the wall and the bubble with the bubble reduces the maximum radius compared to the case where the effect of the impact is not considered and also reduces the amount of erosion. The possible place of erosion is located at the end of the cavitation cavity, and possible damage can be prevented by strengthening this place. The results were compared with other published works and had acceptable accuracy.

1. Introduction

According to the phase diagram of water, cavitation occurs when the local pressure in the liquid is lower than the vapor pressure at the same temperature [1]. Erosion caused by cavitation causes serious damage to parts that are exposed to cavitation, such as hydrofoils, propellers, pumps, fuel injection nozzles and etc. However, this phenomenon also has benefits that are used in many industrial, medical and chemical processes.

In the perusal of bubble dynamics, the study of the interaction of bubbles during cavitation has attracted much attention due to its many applications in various sciences. Despite various studies on the interactive effect of bubbles on each other, the effect of the presence of bubbles on the emitted wave power has been less studied in research, which is one of the innovations of this research.

Ochiai et al. [2] used Eulerian and Lagrangian approaches to evaluate erosion and they tried ranges of cavitation numbers and showed that the highest energy occurs for the cluster of bubbles and near the cavitation cavity. Rasthofer and his colleagues [3] simulated large-scale supercavitation collapse using the Eulerian-Lagrangian model and they found that the speed of the microjet and the oscillation frequency of the bubbles depend on the strength of the collapse wave and therefore depend on the radial position of the bubbles

[Downloaded from ijmt.ir on 2026-11-23]

in the cloud. Using a one-way method, Paquette et al. [4] investigated the collapse of a single air bubble near a deformable wall due to the impact of high pressure waves and they came to the conclusion that this method is unable to show the deformation of the wall and accurately predict the incoming force and an alternative to this method is two-way method.

Fabian Diner [5] has systematically studied the hydrodynamic mechanisms governing the collision of a rising bubble with a solid wall in a creeping flow regime. His results show that the collision of the bubble with the solid wall in the creeping flow regime is controlled by the balance of viscous stresses and surface tension, while the inertia of the bubble has little effect. Because the behavior of a bubble during film drainage is quasi-stationary, the findings associated with film drainage also apply to bubble-wall collisions outside the remit of the creeping flow regime. In the numerical simulation of bubble interactions, Li et al. [6] studied the treatment of two bubbles under the influence of hydrodynamic cavitation and heeded changes in radius growth and swing time compared to the single bubble state. Liang et al. [7] also studied the treatment of two bubbles under the influence of acoustic cavitation and realized the important role of two factors: the ratio of the radius of the bubbles and the ratio of their distance on the behavior of the bubbles.

Raufi et al. [8] developed a numerical scheme for the bubble track that includes their collision. They used the hard-sphere collision model to collide the bubbles. They traced the track of tiny bubbles with the collision and studied the rate of collision and bubble settling.

Heitkom et al. [9] proposed a straightforward model for small bubbles whose simulation is specific to the Lagrangian calculations of bubbles and soft spheres. They studied the impact of a small bubble with an inclined top wall theoretically and empirically. Figure 1 shows the good accuracy of this model with laboratory results. In the present research, the model offered by Heitkom et al. was used to collide a bubble with a wall and two bubbles.

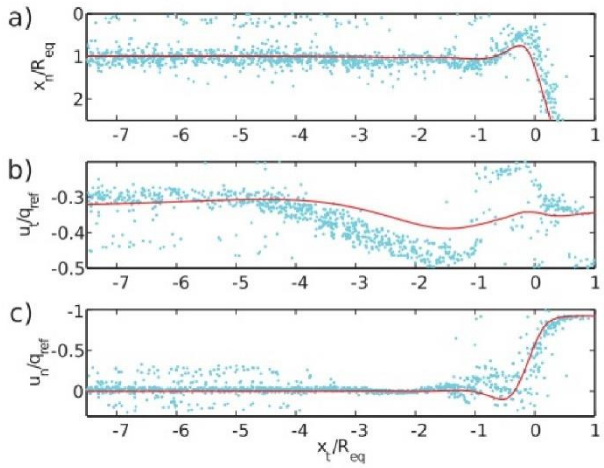


Figure 1. Empirical (points) and numeric (line) results of vertical position (a), tangential velocity (b) and vertical velocity (c) of a bubble with Req = 0.6 mm, colliding with a plane, inclined by αw = 20, as a subordinate of the tangential situation. [9]

The main motivation of this research, with a deeper and more detailed understanding of the phenomenon of erosion and the impact of bubbles, is that using a completely numerical approach based on computer simulations, the need to use experimental and often expensive results can be eliminated, especially for marine industries. Combining Eulerian and Lagrangian viewpoints and using it to better understand the erosion phenomenon, identifying vulnerable areas, investigating the interaction between bubbles and comparing it with the single-bubble state is one of the achievements of this research.

2. Numerical method

Ochiai et al. [2] used the Eulerian and Lagrangian approaches to assess erosion, the propagating pressure wave from the collapse of the cloud cavitation is considered as the main mechanism of damage. According to this model, first, the flow around the desired geometry is solved macroscopically (Eulerian) without considering the dynamic details of the bubble behavior and information about the pressure field and velocity in the desired geometry is obtained. Then, the exact behavior of the particles is examined microscopically (Lagrangian) and with the help of existing functions to evaluate the intensity of the propagated pressure wave, an estimate of the amount and possible location of erosion on the desired geometry is obtained. In this research, the model presented by Ochiai is used.

The proposed numerical prediction method consists of the following processes:

Eulerian approach (by Fluent software):

1- Calculating the flow field around the hydrofoil and determining the pressure and velocity field for all calculation cells(equations 1 and 2).

Lagrangian approach (by Matlab software)

[Downloaded from ijmt.ir on 2026-11-23]

2- Coupling the equations of oscillation and motion and bubble release near the attack edge of the hydrofoil using the fourth-order Runge-Kutta method with variable time step (Equation 16)
3- Applying the obtained pressure and velocity field to the bubble and determining the new values of the radius and location of the bubble (solving equations 3 and 4)
4- Measuring the position of the bubble relative to the suction surface of the hydrofoil and applying the collision condition if needed (solving equations 8, 11 and 12)
5- Repeat steps 3 and 4 until the bubble comes out of the cavity.
6- Evaluation of erosion intensity based on the history of bubble behavior along the track of movement on the surface of the hydrofoil (solving equation 20)

2.1. Numerical method related to cavitation flow

The mixture model is used to simulate two-phase flow. In this model, the flow behaves as a homogeneous mixture of two incompressible and isothermal phases.

$$\frac{\partial}{\partial t}(\rho_m) + \nabla.(\rho_m V_m) = 0 \quad (1)$$

$$\frac{\partial}{\partial t}(\rho_m V_m) + \nabla.(\rho_m V_m V_m) = -\nabla P + \nabla.\left[\mu_m\left(\nabla V_m + \nabla {V_m}^T\right)\right] + \rho_m g \quad (2)$$

In this equation, P &V_m are homogeneous flow pressures and velocities, ρ_m are mixed densities, and μ_m are mixed viscosities.

2.2. Numerical method related to cavitation bubble

2.2.1. Simulation of bubble oscillations

The treatment of the bubble arises from the pressure gradient caused by the flow. The modified Rayleigh-Plesset-Keller-Herring equation [10-11] considers the compressible behavior of the bubble as the bubble collapse velocity approaches the speed of sound, as well as the slip velocity between the bubble and the moving liquid. The items mentioned are not usually used in previous articles. The general form of the equation is as follows:

$$\left(1-\frac{\dot{R}}{c}\right)R\ddot{R} + \left(\frac{3}{2}-\frac{\dot{R}}{2c}\right)\dot{R}^2 = \frac{1}{\rho}\left(1+\frac{\dot{R}}{c}+\frac{R}{c}\frac{d}{dt}\right)\left[P_v + P_{g0}\left(\frac{R_0}{R}\right)^{3K} - P_\infty - \frac{2\gamma}{R} + \frac{4\mu}{R}\dot{R}\right] + \frac{1}{4}(U_f - U_b)^2 \quad (3)$$

In the above equation γ, ρ, c and μ are the surface stress, the density, and the velocity in the liquid, and the viscosity, respectively. $\ddot{R}$, $\dot{R}$ & R are bubble acceleration, wall velocity, and radii, respectively. P_v is the vapor pressure and P_{g0} is the initial bubble pressure. U_{avg} and P_{avg} will be the velocity and mean pressure around the bubble and U_b is the bubble velocity. The coefficient K is the polytropic coefficient of the gas.

2.2.2. Simulation of bubble movement

The motion of the bubble is simulated according to the second equation of Newton's law. Using the discrete phase model (DPM), the fluid is considered as a continuous medium, while the discrete phase is solved by tracing a large number of particles in the calculated flow field. Maxey and Riley presented the bubble motion equation, which exerts the following forces: [12]

$$\rho_b \forall_b \frac{d\overrightarrow{U_b}}{dt} = \forall_b(\rho_b - \rho)g\vec{j} + \forall_b\overrightarrow{\nabla p} + \frac{1}{2}\rho A_b C_d\left(\vec{U} - \overrightarrow{U_b}\right)\left|\vec{U} - \overrightarrow{U_b}\right| + \frac{1}{2}\rho\forall_b\left(\frac{d\vec{U}}{dt} - \frac{d\overrightarrow{U_b}}{dt}\right) \quad (4)$$

In the above equation, index b is related to bubbles and the rest is related to moving fluid. $\forall_b$ the volume of the bubble is $\frac{4}{3}\pi R^3$ and A_b the bubble surface is πR^2. C_d is the drag coefficient obtained experimentally by Haberman and Morton [13]:

$$C_d = \frac{24}{Re_b}\left(1 + 0.197{Re_b}^{0.63} + 2.6 \times 10^{-4}{Re_b}^{1.38}\right) \quad (5)$$

Where Re_b is the Reynolds number of the bubble:

$$Re_b = \frac{2R\left|U_{avg} - U_b\right|}{\vartheta} \quad (6)$$

ϑ is kinematic viscosity. The forces of the right-hand side of the equation are the buoyancy force, the pressure gradient force, the drag force, and the added mass force created by the acceleration of the bubble in the fluid, respectively.

2.2.3. Simulation of a bubble collision

The formulas presented in this section are designed specifically for the Lagrangian calculations of bubble track. This force is only related to the location and speed of the bubble. In this model, no experimental parameters are used to calibrate the results and they are explicit, so it reduces the computational volume. The hydrodynamic forces acting on the bubble and the wall and the two bubbles colliding are 1- Vertical elastic force, 2- Vertical viscous force, 3- Tangential viscous force. For the collision of two bubbles, due to the symmetry of the tangential force, the vertical viscous-elastic model has been used, therefore, the tangential viscous force has not been taken into account in the calculations. Figure 2 is a schematic of the proposed model.

[Downloaded from ijmt.ir on 2026-11-23]

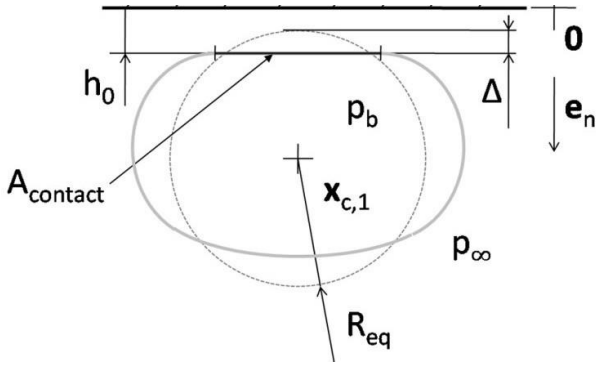


Figure 2 Schematic of the collision of a spherical bubble with an obstacle (wall and deformed bubble) in the collision model [9]

2.2.3.1. Vertical elastic force

The vertical elastic forces due to the change in the superficial energy of the bubble are due to the deformation of the bubble when it collides with another bubble. Therefore, it can be obtained by calculating the bubble shape during the collision proceeding.

$$F_{elastic} = \frac{dE_s}{d\Delta} = \gamma \frac{dA}{d\Delta} \quad (7)$$

The final shape of the elastic force, which includes the bubble position, the bubble radius, and the surface tension, is as follows:

$$F_{elastic} = \gamma R_{eq}(18.5\left(\frac{\Delta}{R_{eq}}\right)^2 + 2\frac{\Delta}{R_{eq}}) \quad (8)$$

In the above formula Δ is the overlap distance shown in Figure 2. To calculate this distance, we use the following equation:

$$\Delta = R_{eq} - \frac{1}{2}|x_{c,1} - x_{c,2}| + \frac{h_0}{2} \quad (9)$$

h_0 is the thickness of the liquid film between the two bubbles. The following equation is used to calculate this thickness:

$$h_0 = \sqrt{\frac{3}{16}}\sqrt{\mu U_b \frac{{R_{eq}}^2}{\gamma}} \quad (10)$$

2.2.3.2. Vertical viscous force

To obtain this force, it is first necessary to obtain the flow between the two bubbles and then to examine the shape of the layer between the two bubbles, which is a very complex problem. For this purpose, a simple analytical method is proposed based on the condition that there is no slipping between the bubble surfaces and that tangential motion does on average not efficacy the waste caused by the normal motion:

$$F_{viscous} = 0.65 U_b C_{bc} \mu \left(\frac{\Delta}{R_{eq}}\right)^{-0.5} (4\sqrt{\frac{{R_{eq}}^3}{h_0}} + \frac{3}{2}\frac{{R_{eq}}^2}{h_0}) \quad (11)$$

C_{bc} is the collision parameter that is equal to 1/4. In the case of a bubble colliding a wall, this parameter is equal to 1.

2.2.3.3. Tangential viscous force

An additional frictional force acting on the bubble, when a bubble moves parallel to the wall. Goldman et al. [14] suggested the following equation for this force:

$$F_{tang} = \frac{16}{5}\pi U_b \mu R_{eq} ln(\frac{\delta}{R_{eq}}) \quad (12)$$

δ the distance between the bubble and the wall can be obtained from the following equation:

$$h_0 = \sqrt{\frac{3}{8}}\sqrt{\mu U_b \frac{{R_{eq}}^2}{\gamma}} \quad (13)$$

The above equation is also used to calculate the thickness of the liquid film between the bubble and the wall. If, if the bubble does not collide with the wall but glides along the wall, the value of 10 micrometers is selected as the minimum normal thickness of the liquid film [15] and when the bubble moves away from the wall, δ is greater than R_{eq} and no tangential viscous force is applied automatically. By adding these forces to Equation (4), practically after examining the collision condition, these forces are applied and correct the radius and direction of movement of the bubble.

In the collision of the bubble with the wall, it has been done in such a way that if the distance between the center of the bubble and the wall is less than the radius of the bubble, the condition of collision with the wall is considered and if the distance from the center of the bubble to the wall is less than the radius of the bubble plus the value of ε, which is greater than the thickness of the liquid film between the bubble and the wall, the bubble will slide along the wall.

The condition of bubble collision in the hard-sphere collision model [16] is that when the distance between the center of two bubbles is equal to the sum of the radii of the two bubbles, the collision takes place. In the case of a bubble colliding with another bubble due to a change in the radius of the bubble in the research, this condition has been modified as follows:

$$\frac{dist}{R_1 + R_2} \leq 1 \quad (14)$$

Equation (14) operates in such a way that when in a time step the distance between the centers of two bubbles is less than or equal to the sum of the radii of both bubbles in the same time step, the collision forces are applied in the main equation and the equation is modified.

2.2.4. Solve the differential equation and variable time step

Equations (3) and (4) form a set of ordinary differential equations (ODE). To solve this equation, the fourth-order Runge-Kutta method with variable time step has been used. Using the variable time step has greatly reduced the speed of solving this equation. As Hairer and Wanner (1991) point out, the PID controller can be used to solve time steps to solve ODE equations. In this method, the e_n function is defined to change the radius [17]:

[Downloaded from ijmt.ir on 2026-11-23]

$$e_n = \frac{|R^n - R^{n-1}|}{R^n} \quad (15)$$

Where R^n and R^{n-1} are the radii of the bubble in the time step n and n-1, respectively. The next time step to control e_n is calculated:

$$\Delta t_{n+1} = C_{dt}\Delta t_n = \left(\frac{e_{n-1}}{e_n}\right)^{K_p}\left(\frac{TOL}{e_n}\right)^{K_l}\left(\frac{{e_{n-1}}^2}{e_n e_{n-2}}\right)^{K_d}\Delta t_n \quad (16)$$

Where K_p, K_l and K_d are constants of proportionality, integral and controller derivative and their values are "0.075", "0.0175" and "0.01", respectively. The value of TOL varies depending on the circumstances of the problem, the number "0.01" has given acceptable answers for the subject under study.

2.3. Numerical method related to cavitation erosion intensity

After passing through the low-pressure zone and bubble growth, environmental pressure causes the bubble to collapse. Shock waves are emitted into the fluid during the collapse process. Shock waves cause impulsive pressure and damage the surface of the material, causing surface erosion.

According to the equation offered by Soyama et al. [18], the energy from each collision is calculated as below:

$$E_i = I_i \tau_i A_i = \frac{{P_i}^2}{2\rho c}\tau_i A_i \quad (J) \quad (17)$$

I_i , τ_i , and A_i are acoustic energy, duration, and effective area, respectively. P_i is the collision pressure on the wall surface, which is obtained from Equation (18).

$$P(r,t) = P_0 + \rho\left(-\frac{\acute{f}}{r} - \frac{f^2}{2r^4} - \frac{1}{2c}\left(\frac{\acute{f}^2}{cr^2} + \frac{2f\acute{f}}{r^3}\right)\right) \quad (18)$$

$f = -R^2\dot{R}$ and $\acute{f}$ are derivatives of the function f. [19] If we assume the elements ρ, c, and τ_i to be constant, the following relation is extracted by integrating the obtained expression:

$$E_i \propto {P_i}^2 A_i = \int {P_i}^2 dA \quad (19)$$

Finally, the total energy of cavitation shocks, which is the result of the accumulation of all shocks on each other, is obtained from the following equation:

$$\mathrm{E} = \sum E_i \propto \sum \int {P_i}^2 dA \quad (20)$$

3. Results and Discussion

The flow and motion of the bubble around the two-dimensional NACA0015 hydrofoil with a chord length of 70 mm were investigated and the C-type grids were placed around the hydrofoil. The applied boundary conditions are 10 m/s inlet velocity with a 7 attack angle and outlet pressure for hydrofoil. Fluid contact with non-slip hydrofoil walls is considered. The SIMPLE algorithm is used for pressure and velocity coupling.

3.1. Numerical model validation

To be accurate in the numerical model used in both Eulerian and Lagrangian contexts, this validation has been done.

3.1.1. Eulerian part validation

For accuracy in the simulation, the numerical results are compared with the experimental results of Van Rijsbergen and Boorsma [20] for NACA0015 hydrofoil, which has good accuracy.

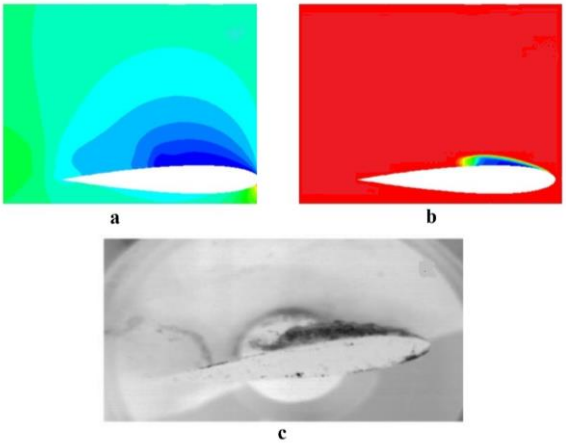


Figure 3 Comparison of a) Pressure distribution and b) Liquid volume fraction distribution with c) Experimental results for NACA0015 hydrofoil [20]

Independence from the network was checked for three organized networks with 30350, 78600 and 156500 nodes, and in the results obtained in the table below, not many changes were observed with these three networks, therefore, to be sure, the second network was chosen to continue the investigations. The use of this type of network significantly reduces the calculation time and improves the convergence of the problem. In the areas close to the wall, the boundary layer grid has been used in order to see the gradients as well as possible.

Network number	Number of nodes	lift coefficient	Drag coefficient
1	30350	0.315	0.0399
2	78600	0.318	0.0417
3	156500	0.323	0.0428
		2.53 % Network error percentage 1 and 3	7.26 % Network error percentage 1 and 3

3.1.2. Lagrangian part validation

To ensure the validity of the results in predicting bubble treatment, the simulated results of bubble treatment are compared with the empirical data of Flannigan et al. [21]. Figure 4 shows the radius changes of an argon gas bubble in 85% sulfuric acid with an initial radius of

[Downloaded from ijmt.ir on 2026-11-23]

$R_0 = 13\mu m$. The conditions governing the problem are $k = 1.67, \mu = 0.02036 \frac{kg}{ms}, \sigma = 0.055 \frac{N}{m}$ and $\rho = 1714\ kg/m^3$. This bubble is under the sine wave of excitation $P_{ex} = -P_a \sin(2\pi f t)$ with excitation amplitude $P_a = 1.42 P_0$ and initial pressure $P_0 = 1\ atm$ and excitation frequency $f = 28.5\ kHz$. As can be seen, there is a good correlation between the results of the numerical solution and the experimental values at the stage of bubble growth, collapse, and first oscillation, so that the error rate in the maximum diagram is 2.3%. However, in the continuation of the rebounds, the experimental values of dumping showed more. The reason for this can be related to factors such as chemical reactions, and the effects of heat transfer and mass transfer that have not been studied in the current section [22].

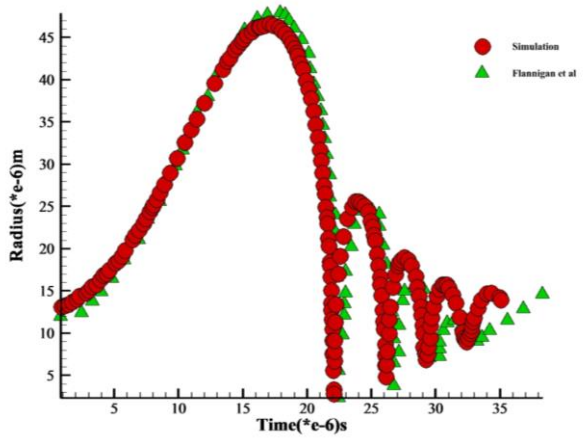


Figure 4 Comparison of Argon Bubble Behavior in Sulfuric Acid with Experimental Results of Flannigan et al.

3.2. Investigation of cavitation flow

In this section, bubble behavior for different cavitation numbers is investigated. Every flow, whether cavitation or non-cavitation, has its cavitation number. Generally, in the study of cavitation number for a certain amount of cavitation number, cavitation phenomenon occurs and in industrial applications, finding this number is very important, so this phenomenon can be controlled by studies. Given that the pressure distribution in cavitation numbers is varied and that the growth and collapse of bubbles are due to the pressure gradient, we expect the bubbles to behave in proportion to the pressure. Figure 5 shows the pressure distribution for each of the cavitation numbers.

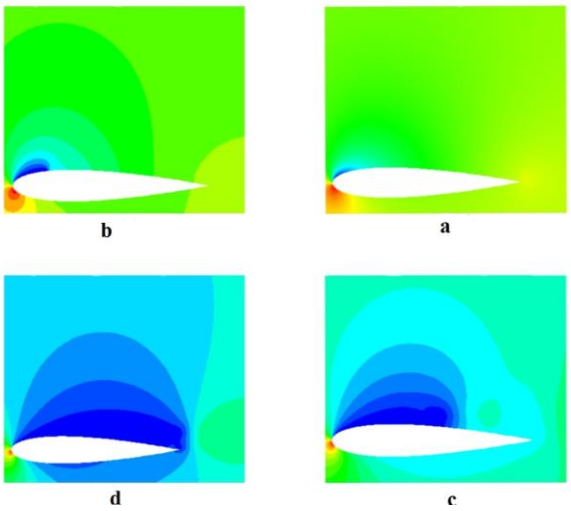


Figure 5 Pressure distributions for a) $\sigma = 2$, b) $\sigma = 1.6$, c) $\sigma = 0.64$ and d) $\sigma = 0.4$

In this regard, cavitation numbers 0.4, 0.64, 1.6, and 2, each of which has specific conditions of cavitation, have been selected. In Figure 3-3 (a) single-phase flow, Figure 3-3 (b) cavitation inception occurs. In Figure 3-3(c) cloud cavitation and Figure 3-3(d) super cavitation will be observed.

3.3. The effect of cavitation number on the bubble colliding with the wall

What is expected is that the bubble should behave differently in different conditions, therefore, at first, the effect of cavitation number in the case of the effect of collision with the wall is not considered, for the initial radius of 100 μm. In Figure 6 , the vertical axis is the ratio of the bubble radius to the initial radius and the horizontal axis is the chord length in the bubble track. In this case, a 13-fold increase in radius is observed for $\sigma = 0.4$. For $\sigma = 0.64$ this increase is seen to be 9.4 times and for $\sigma = 1.6$, 4 times increase. For cavitation number 2, due to the decrease in pressure at the leading edge, an increase of approximately 2 times has occurred, but it collapses in the same range and oscillate around its initial radius.

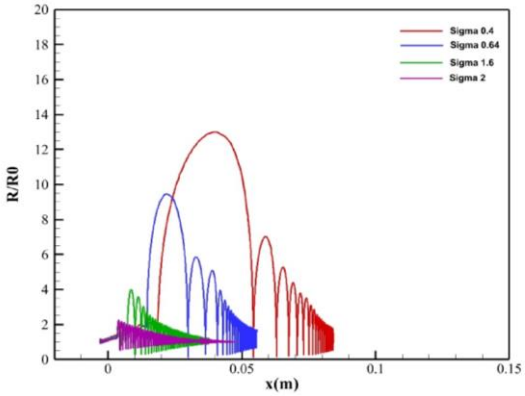


Figure 6 Graph of radius changes along the bubble motion track for different cavitation numbers for an initial radius of 100 µm

[Downloaded from ijmt.ir on 2026-11-23]

By considering the effect of the bubble colliding with the wall at different cavitation numbers, Figure 7 is obtained.

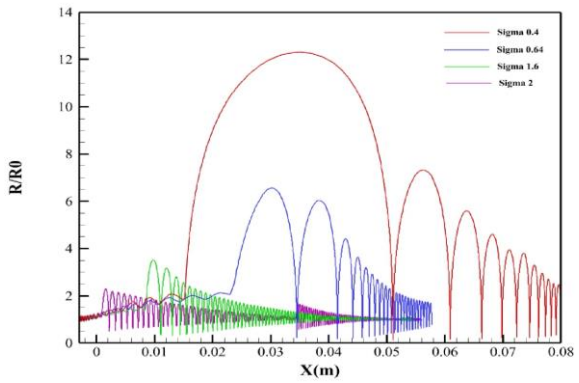


Figure 7 Graph of radius changes after colliding with a wall along the bubble travel path for different cavitation numbers for an initial radius of 100 µm

The rate of increase of the radius in the cavitation number $\sigma = 0.4$ is 12.2 times the initial radius. For $\sigma = 0.64$, this increase is seen to be 6.5 times and for $\sigma = 1.6$, an increase of 3.1 times. For cavitation number 2, an increase of approximately 2 times is seen as in the previous case.

By comparing the diagrams of Figure 6 and Figure 7, the following results are obtained:

A) The effects of increasing the radius by decreasing the cavitation number are the same, when the bubble colliding with the wall is applied and when it is not. Therefore, as the cavitation number increases, the growth of the bubble radius decreases.

B) The maximum radius in the case of impact with the wall is reduced to the state of non-impact with the wall.

C) The process of bubble growth starts earlier in the case of a collision with the wall than in the case in which the collision did not occur, therefore, the cavitation number has little effect in this case and is related to the impact effects.

3.4. The effect of the initial radius on the collision of the bubble with the wall

Since the effect of cavitation number on the impact effect is the same as not on it, the effect of the initial radius on the impact of the bubble on the suction side of hydrofoil is investigated below, therefore, variable bubbles with initial radii of 50 µm, 100 µm and 200 µm in the same coordinates are dropped for $\sigma = 0.64$. Figure 8 shows the radius of the bubble before it hits the wall and after it hits the wall with an initial radius of 50 µm. As shown in Figure 8 , the radius of the bubble did not change significantly after colliding with the wall, and the reason for this is that the bubble did not collide with the surface of the hydrofoil and the condition of colliding the wall did not affect this condition. For a better view of these conditions, the track of bubble movement before impact and after impact with the wall is shown in Figure 9.

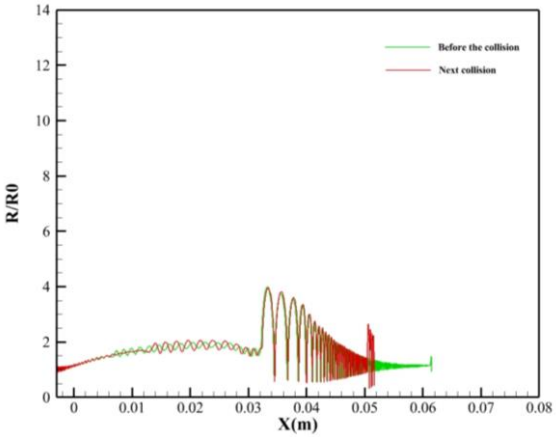


Figure 8 Bubble radius before and after impact with a wall with an initial radius of 50 µm.

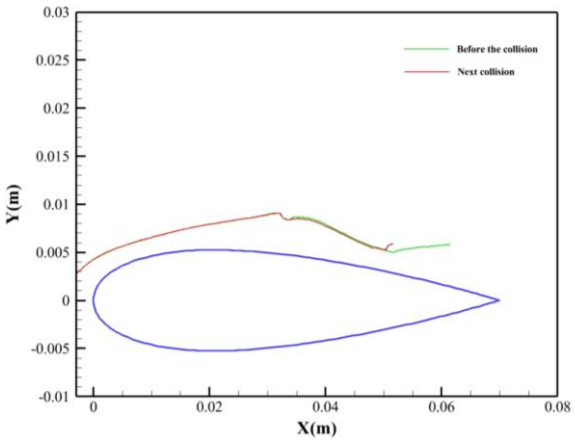


Figure 9 Track of bubble before and after impact with a wall with an initial radius of 50 µm.

Figure 10 shows the bubble radius before and after colliding the wall with an initial radius of 100 µm.

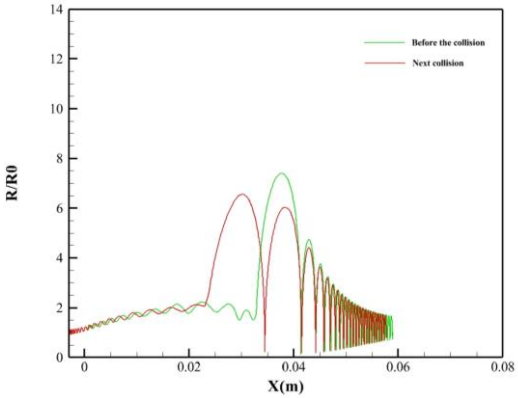


Figure 10 Bubble radius before and after impact with the wall with an initial radius of 100 µm.

[Downloaded from ijmt.ir on 2026-11-23]

According to Figure 10, the maximum reduction of the radius compared to before the collision is about 11%. The forces applied due to the impact with the wall, especially the tangential viscous force, have caused the growth of the bubble radius to occur earlier than before the collision. Figure 11 shows the track of the bubble before it collides and after it collides with the wall.

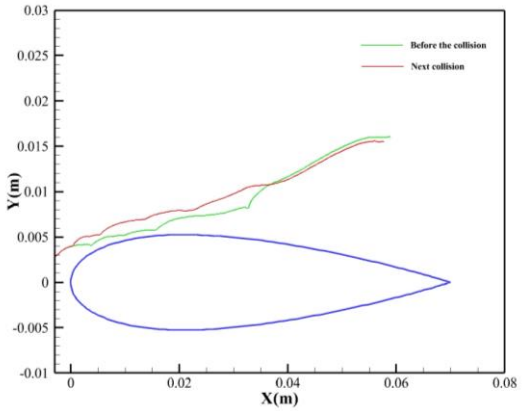


Figure 11 Track of bubble before and after impact with a wall with an initial radius of 100 µm.

To complete this section, a bubble with an initial radius of 200 **µm** is released and the effects of a collision with the wall and the track are shown in the following diagrams. The maximum radius reduction, in this case, is about 33% and as before, the bubble starts to grow earlier than when the wall has not been colliding.

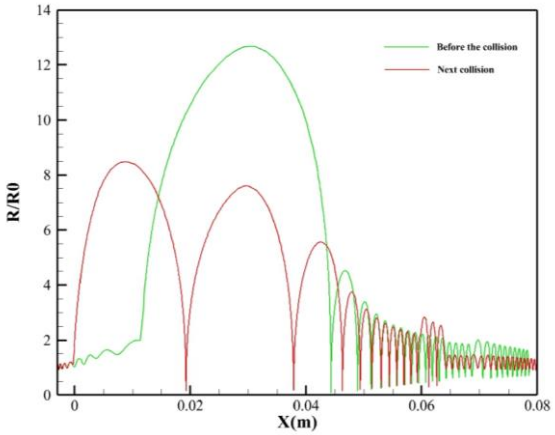


Figure 12 Bubble radius before and after impact with the wall with an initial radius of 200 µm.

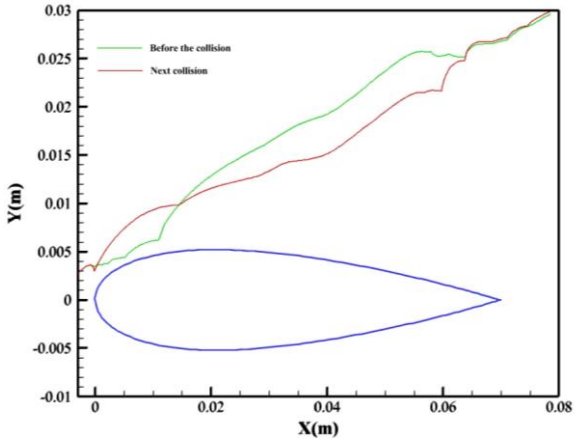


Figure 13 Track of bubble before and after impact with a wall with an initial radius of 200 µm.

Also, the bubbles fluctuate more after colliding the wall, which is not far from expected, however, after the bubble collapses, the bubble fluctuations are almost the same as before, which indicates that the effects of the impact after the collapse do not apply to the bubble anymore.

3.5. Effect of initial radius on bubble collision with adjacent bubble

To check the bubble radius and better compare the single bubble mode is also given for accurate comparison. As shown in Figure 14, the largest bubble radius growth is related to the single bubble state. By putting up a bubble with a smaller radius (**50µm**) in the vicinity of the bubble (100 **µm**), there is no change in the bubble radius, this means that there is no collision between the two bubbles and it is not different from the single bubble state, so the bubble radius has not changed. As the initial radius of the adjacent bubble increases, its effect on the behavior of the bubble also increases, so that by putting up the bubble with an initial radius of 100 **µm** in the vicinity of the bubble (100 **µm**), the maximum radius is reduced by about 9%. By putting up the bubble with an initial radius of **200µm** in its vicinity, the maximum value of the radius is reduced by about 26%. Also, it can be seen that the minimum value of the radius after the collapse in four cases is not significantly different from each other and it can be said that this value is independent of the radius of the adjacent bubble.

[Downloaded from ijmt.ir on 2026-11-23]

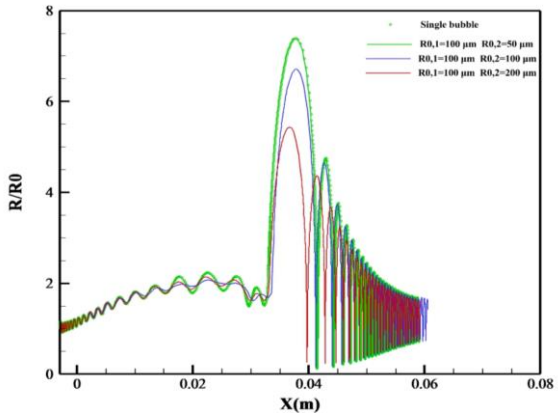


Figure 14 Comparison of bubble radius in the collision of two bubbles in a single state and the presence of bubble with initial radii of 50 µm, 100 µm, and 200 µm.

Adjacent bubble Since it is at the top of the bubble, we expect it to tilt towards the wall after the bubble collides. To better understand the track of the bubble after the collision is also drawn. Figure 15 shows the trajectory of the bubble before colliding with the bubble with an initial radius of 100 **µm** and after colliding with the bubble. According to Figure 15, the deflection of the track occurred in the range of 0.01 after the leading edge of the hydrofoil. Figure 16 shows the trajectory of the bubble before colliding with the bubble with an initial radius of 200 **µm** and after colliding with the bubble. According to Figure 16, the deflection of the track occurred near the zero range after the leading edge of the hydrofoil. The amount of deflection at the end of the track in the pre-collision state (y = 0.016) with the state where the adjacent bubble has an equal radius (y = 0.156) is less than the state where the adjacent bubble has a radius greater than the initial radius (y = 0.014).

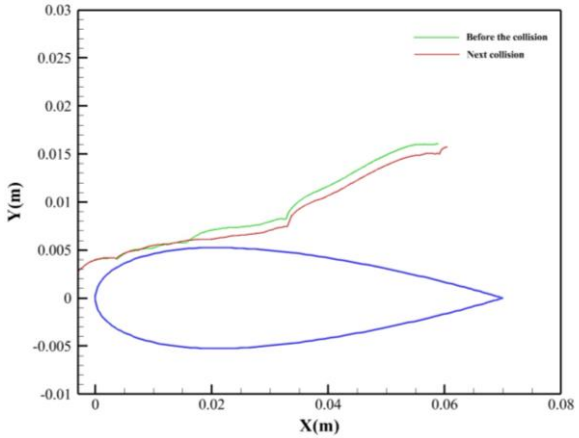


Figure 15 Track of a bubble with an initial radius of 100 µm before and after colliding with another bubble with an initial radius of 100 µm

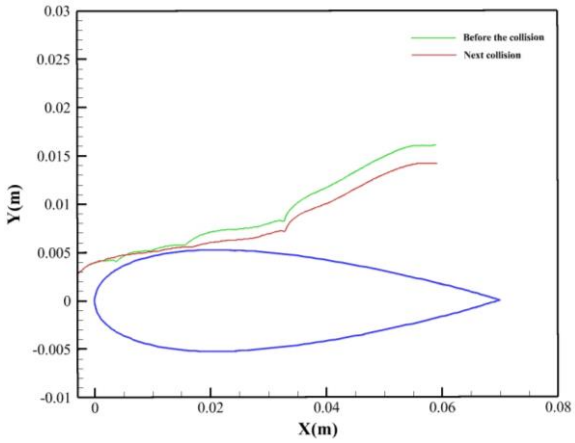


Figure 16 Track of a bubble with an initial radius of 100 µm before and after colliding with another bubble with an initial radius of 200 µm

3.6. Investigation of erosion after the collision

3.6.1. Investigation of erosion after collision with the wall

To investigate the erosion effect, three groups of 10 bubbles were left near the leading edge to study the erosive effects of the collision with the suction side of the hydrofoil. To better compare the effects of post-impact erosion, first pre-collision erosion and post-impact erosion are shown for a bubble group with an initial radius of 100 µm, and finally, three groups of released bubbles are compared. The maximum amount of erosion diagrams (Figure 17) for the group of 10 before the collision (1.97e13) and after the collision (5.79e12) is about 3.5 times less than before the collision.

As expected, with increasing initial radius, the erosive effects increase as shown in Figure 18. The interesting point in this diagram is the existence of two peaks in the initial radius of 200 µm, the first peak is in the range of 0.022 m and the second peak is in the range of 0.047 m. The peak range for other radii is in the second peak range with an initial radius of 200 µm. This may be because the bubbles may collapse several times along the trajectory of the pressure gradient they encounter, the existence of the second peak is due to the re-collapse of some bubbles, which also experience a lot of fluctuations in this bubble radius.

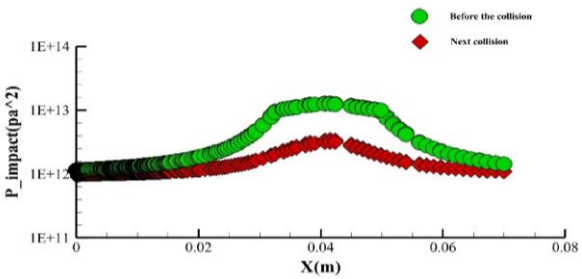


Figure 17 Prediction of erosion before and after impact with the wall on the suction side of the hydrofoil for bubble handle with initial radius 100 µm

[Downloaded from ijmt.ir on 2026-11-23]

The maximum amount in the diagram in Figure 18 is related to the radius of 200 µm (4.2e13) 7.25 times higher than the maximum erosion related to the radius of 100 µm (5.79e12) and 42 times higher than the maximum erosion related to the radius of 50 µm (1e12). By comparing the erosion diagram for the single bubble mode and the collision mode, we see a decrease in the amount of erosion for the wall collision mode.

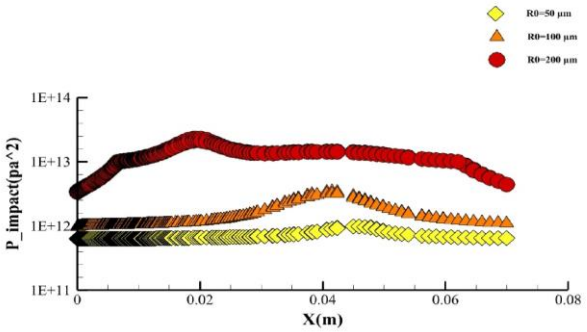


Figure 18 Prediction of erosion after impact with the wall on the suction side of the hydrofoil for bubble handle with initial radii a) 50 µm, b) 100 µm and c) 200 µm

3.6.2. Investigation of erosion after collision with adjacent bubble

Due to the change in bubble radius after the collision, it is expected that this change in bubble behavior will cause changes in bubble erosion. As before, three groups of 10 bubbles are dropped near the leading edge of the hydrofoil and because the state of the adjacent bubble, which was smaller than the initial radius, did not differ from that of the single bubble, this state is taken into account in the calculations of single bubble erosion.

Figure 19 shows the sum of the impact forces applied to the suction side of the hydrofoil by the size of the bubbles for $\sigma = 0.64$. As shown in Figure 19, as the initial radius of the adjacent bubble increases, its effect on the main bubble increases. The erosion power of adjacent bubbles with an initial radius of 200 µm is approximately 10 times less than the erosion power of adjacent bubbles with a radius of 100 µm and a single bubble state. The erosion power of a single bubble is slightly different from that of a bubble adjacent to an initial radius of 100 µm, thus, the maximum of the adjacent bubble diagram (1.26e13) is 36% lower than the single bubble diagram (1.97e13).

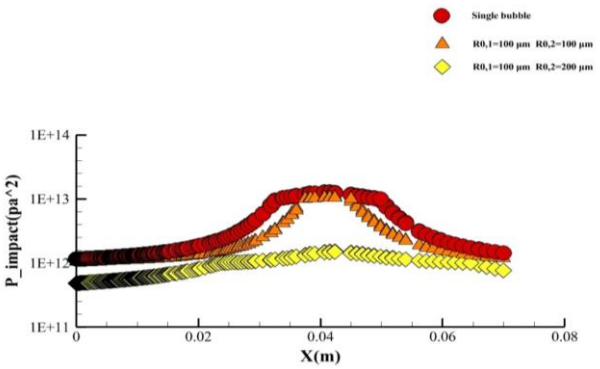


Figure 19 Prediction of erosion on the suction side of the hydrofoil for single bubble mode and adjacent bubble mode.

3.6.2. Investigation of erosion site

Ochiai et al. [25] also in an article that investigated the rate of holes caused by erosion on the NACA0015 hydrofoil. They came to the conclusion that the most probable place is between 60-80 percent of the chord length, which is in relatively good agreement with the research results. According to figure 3-b, the length of the cavity is approximately equal to 0.38m of the length of the chord. The maximum location of the erosion graphs shows the probability of the highest place for erosion, which according to the graph is located at the end of the cavitation hole. Therefore, it is possible to predict the place of erosion with great accuracy in both collision situations to prevent possible injuries.

4. Conclusion

The effects of the bubble collision were investigated on NACA0015 hydrofoil using the Eulerian-Lagrangian perspective. Using the fourth-order Runge-Kutta method, we were able to combine the Eulerian view with the Lagrangian view, and using the variable time step greatly speeds up the solution. Erosion caused by bubble collision under the influence of two factors of cavitation number and initial radius was investigated and the following results were obtained:

1- Considering the effects of a collision, the growth rate of the radius is less than in the case where this effect is not taken into account.
2- The rate of erosion for the bubble handle with an initial radius of 100 µm after impact with the wall is 3.5 times less than before the impact.
3- With the increase of the initial radius in collision with the wall, the amount of erosion has increased so that the erosion related to the 200 µm radius is 7.25 times more than the 100 µm radius and 42 times more than the 50 µm radius.

[Downloaded from ijmt.ir on 2026-11-23]

4- By increasing the initial radius of the adjacent bubble compared to the desired bubble (100 μm), the effect of the larger adjacent bubble (200 μm) on the erosion of the desired bubble has increased and the erosion rate has decreased by nearly 10 times compared to other cases.
5- In order to prevent the possible damage caused by erosion, it is necessary to strengthen the possible places, which will be the area at the end of the cavity hole, the area with the highest risk of erosion.

5. References

[1] Franc, J.-P., Michel, J.-M., (2006), *Fundamentals of cavitation*, Springer Science & Business Media, doi:10.1007/1-4020-2233-6

[2] Ochiai, N., (2009), *Numerical Prediction of Cavitation Erosion in Cavitating Flow*, Proceedings of the 7th International Symposium on Cavitation CAV2009, Paper No. 67.

[3] Rasthofer, U., Wermelinger, F., Karnakov, P., Sukys, J. and Koumoutsakos, P., (2018), *A Computational Study of the Collapse of a Cloud with 12500 Gas Bubbles in a Liquid*,

[4] Paquette, Y., Fivel, M., Ghigliotti, G., Johnsen, E. and Pierre, J., (2019), *Fluid-Structure Interaction in Cavitation Erosion*, HAL Id: hal-02066203.

[5] Fabian, D., (2018), *Wall collision of deformable bubbles in the creeping flow regime*, European Journal of Mechanics / B Fluids, doi:10.1016/j.euromechflu.2018.02.002.

[6] Li, F., Cai, J., Huai, X. and Liu, B.,(2013), Interaction mechanism of double bubbles in hydrodynamic cavitation, J.Therm. Sci. 22, p.242-249, doi:10.1007/s11630-013-0619-9.

[7] Liang, J., Han, G., Fengbin, L. and Darong, C., (2016), *Investigations on Dynamics of Interacting Cavitation Bubbles in Strong Acoustic Fields*, Ultrason-Sonochemistry. doi:10.1016/j.ultsonch.2016.05.017.

[8] Raoufi, A., Shams, M. and Ebrahimi, R., (2008), A Novel CFD Scheme for Collision of Micro-bubbles in Turbulent Flow, Engineering Letters, 16:3, EL_16_3_02.

[9] Heitkam, Sommer, A.E. and Drenckhan, W., (2017), *A simple collision model for small bubbles*, Journal of Physics: Condensed Matter, doi:10.1088/1361-648X/aa56fc

[10] Plesset, M.S. and Prosperetti, A., (1977), *Bubble Dynamics and Cavitation*, Annu. Rev. Fluid Mech.9(1), p.145–185, DOI: 10.1146/annurev.fl.09.010177.001045.

[11] Prosperetti, A., and Lezzi, A., (1986), *Bubble Dynamics in a Compressible Liquid*, J. Fluid Mech.168, p.457–478 DOI: 10.1017/S0022112086000460.

[12] Maxey, M. R., (1983), *Equation of Motion for a Small Rigid Sphere in a Nonuniform Flow*, Phys.Fluids.26(4), p.883 DOI: 10.1063/1.864230.

[13] Haberman, W. L. and Morton, R. K., (1953), *An Experimental Investigation of the Drag and Shape of Air Bubbles Rising in Various Liquids*, Navy Dep. David Taylor Model Basin Washington.DC, p.1–55, DOI: 10.5962/bhl.title.47521

[14] Goldman, A. J. and C, R.,(1967), *The Slow viscous motion of a sphere parallels to a plane wall 1 motion through a quiescent fluid*, Chem. Eng. Sci. 22 637–51.

[15] Hendrix, M.H.W. and M, R.D., (2012), *Spatiotemporal evolution of thin liquid films during impact of water bubbles on glass on a micrometer to nanometer scale*, Phys. Rev. Lett. 108 247803.

[16] Hoomans, B.P.B., Kuipers, t. J. A. M., Briels ,W. J. and Van Swaaij, W.P.M., (1996), *Discrete Particle Simulation of Bubble and Slug Formation in a Two-Dimensional Gas-Fluidised Bed: A Hard-Sphere Approach*, Department of Chemical Engineering, Twente University of Technology, P.O. Box 217,7500AE Enschede-99-118.

[17] Hosseininejad, S.S.A., (2016), *CFD Modeling of Cavitation for Fine Particle Flotation*, A thesis submitted in partial fulfillment of the requirements for the degree of Doctor of Philosophy in Chemical Engineering, pp. 83-85.

[18] Soyama, H., Kumano, H. and Saka, M., (2001), *A New Parameter to Predict Cavitation Erosion*, http//resolver. Caltech. edu/cav2001 Sess. 002, p.1-8.

[Downloaded from ijmt.ir on 2026-11-23]

[19] Keller, J.B. & Kolodner, I.I., (1956), *Damping of underwater explosion bubble oscillations*, J. Appl.Phys.271152–1161, doi:10.1063/1.1722221

[20] Van Rijsbergen, M. and Boorsma, A., (2011), *High-speed video observations and acoustic impact measurements on a NACA0015 foil*, CRS EROSION II Working Group, proprietary.

[21] Flannigan, D.J., Hopkins, S.D., Camara, C.G., Putterman, S.J. and Suslick, K.S., (2006), *Measurement of pressure and density inside a single sonoluminescing bubble*, Phys. Rev. Lett. 96, doi:10.1103/PhysRevLett.96.204301.

[24] Cogné, C., Labouret, S., Peczalski, R., Louisnard, O., Baillon, F. and Espitalier, F., (2016), *Theoretical model of ice nucleation induced by acoustic cavitation* , Ultrason. Sonochem.29, doi:10.1016/j.ultsonch.2015.05.038.

[25] Ochiai, N., Iga, Y., Nohmi, M. & Ikohagi, T., (2013), *Study of Quantitative Numerical Prediction of Cavitation Erosionin Cavitating Flow*, Journal of Fluids Engineering., Vol. 135 / 011302-1, DOI:10.1115/1.4023072.

[Downloaded from ijmt.ir on 2026-11-23]